Comparisons of Surface Plasmon Sensitivities in Periodic Gold Nanostructures

Kuang-Li Lee · Way-Seen Wang · Pei-Kuen Wei

Abstract The wavelength sensitivities of three kinds of nanostructures (nanoslits, nanoholes, and concentric circles) with various aperture sizes were compared in water environment. These nanostructures were made on a 110-nm-thick gold film with a period of 600 nm. Surface plasmon resonances in these nanostructures produce transmission dips near the phase-matching conditions while peaks at longer wavelengths. The wavelength sensitivities measured at dips are close to theoretical predictions and about 1.5 times larger than those measured at peaks. Such sensitivity difference is attributed to various surface plasmon distributions, as illustrated by the finite-difference time-domain calculations. In addition, the sensitivity decreases with the increase of aperture size. The nanoslit array and concentric circles have better sensitivities than the nanohole array due to the no cut-off transmission.

Keywords Nanostructures · Surface plasmon resonance · Wavelength sensitivity

K.-L. Lee · W.-S. Wang
Graduate Institute of Photonics and Optoelectronics,
Department of Electrical Engineering,
National Taiwan University,
No. 1, Section 4, Roosevelt Road,
Taipei 10617, Taiwan

K.-L. Lee · P.-K. Wei
Research Center for Applied Sciences, Academia Sinica,
No. 128, Section 2, Academic Road,
Taipei 11529, Taiwan

P.-K. Wei (✉)
Department of Optoelectronics,
National Taiwan Ocean University,
Keelung, Taiwan
e-mail: pkwei@gate.sinica.edu.tw

Introduction

The resonance of surface plasmons (SPR) on gold thin film is widely applied for sensitive and label-free biosensing [1–3]. The widely used method employs attenuated total internal reflection (ATR) in a glass prism to excite the SPR. ATR biosensors are very sensitive to surface environmental changes. However, the ATR setup is typically bulky and requires a large amount of sample solution. Due to its optical configuration, it is hard to be applied for high-throughput and chip-based detections. Recently, excitations of surface plasmons by using metallic nanometer apertures have drawn great attentions and extensive studies. In the case of periodic metallic nano-apertures, the resonances of surface plasmons results in extraordinary transmissions at some certain wavelengths. Those SPR wavelengths are found near the phase-matching conditions of metallic gratings [4–6]. For a normally incident light, the phase-matching condition is described as

$$\lambda(i,j) = \frac{a_0}{\sqrt{i^2 + j^2}} \left(\frac{\varepsilon_m n^2}{\varepsilon_m + n^2} \right)^{1/2} \tag{1}$$

Where i and j are the diffraction orders of gratings in x and y directions, λ is the incident wavelength, a_0 is the period of the nanostructure, ε_m is the dielectric constant of metal and n is the refractive index of surface medium. Since the extraordinary transmission is a result of SPR, it is expected to have good surface sensitivity similar to a conventional SPR sensor [7]. In addition, the typical area of the periodic nanostructure is about 100 μm, same as the spot size of a DNA microarray. Tens of thousands of SPR detection points can be put on a glass slide. Therefore, periodic metallic nanostructures are very suitable for high-throughput and chip-based detections [8–10].

In previous studies, the SPR mode sensitivity of gold periodic nanostructures was measured at the wavelength of enhanced transmission (peak wavelength). It is noted that periodic nanostructures typically produce a transmission peak followed by a dip near the phase-matching condition according to the Fano model [11–13]. Both transmission peak and dip are results of SPR but with different distribution of surface plasmons. The distribution variations at the peak and dip wavelengths may result in different surface sensitivity. Furthermore, the theoretical wavelength sensitivity is calculated directly from the phase-matching condition [9].

$$S = \frac{\Delta\lambda}{\Delta n} = \frac{a_0}{\sqrt{i^2+j^2}} \sqrt{\left(\frac{\varepsilon_m}{\varepsilon_m + n^2}\right)^2} \qquad (2)$$

This equation indicates that SPR mode sensitivity is determined only by the period and the diffraction orders. It is independent of kinds of periodic nanostructures, such as nanoslit arrays or nanohole arrays. The width of nanoslit or diameter of nanohole is also irrelative to the sensitivity. However, it was well known that the aperture size and type of the metallic nanostructures have different contributions in the extraordinary transmission [14–16]. The different surface plasmon behaviors may result in different SPR sensitivities for various nanostructures even with the same period.

In this paper, we first measured and compared the SPR wavelength sensitivities in aqueous conditions for different gold nanostructures with the same 600-nm period. We found that SPR sensitivity measured at dip wavelength is ~600/refractive index unit (RIU), consistent with the predictive value as calculated from Eq. 2. However, the sensitivity measured at peak wavelength is only ~400/RIU, much smaller than the prediction. From finite-difference time-domain (FDTD) calculations, the optical pattern at dip wavelength shows extensive surface plasmons on outside gold surface. On the other hand, the optical profile at peak wavelength has an intense field near the aperture. It reduces the effective SPR area and lowers the sensitivity. Kinds of nanostructure also affect the SPR sensitivity. For the nanoslit array, the transverse-magnetic (TM) incident wave has no cut-off condition [17]. The slit can be as small as several nanometers. The slit width has little effect on the sensitivity. However, light is cut-off in a nanohole. The hole has to be large enough to have enough light transmission. The sensitivity of a nanohole array is thus smaller than that of a nanoslit array.

## Fabrication and spectra measurement

Metallic nanoslits were fabricated by using electron beam lithography and dry etching method. We used a soda lime glass slide as the substrate. A 5-nm-thick Ti film and a 110-nm-thick gold film were sequentially deposited on the glass sample by using an electron gun evaporator. The Ti film was used to provide good adhesion between gold film and glass surface. After the deposition, we used an electron beam writer and a reactive ion etching machine to make the gold nanostructures. Details of the fabrication can be found elsewhere [10]. In the experiments, we designed three kinds of periodic nanostructures: nanoslit arrays, nanohole arrays, and concentric circles. Figure 1a shows the SEM images of different nanostructures on the glass substrate. These arrays have the same 600-nm period and the same 150-×150-μm area. To compare the sensitivities with different aperture sizes, we also fabricated nanoslit arrays with various slit widths (from 20 to 100 nm) and nanohole arrays with various hole diameters (from 90 to 250 nm).

Figure 1b shows the optical setup for measuring transmission spectra of various periodic nanostructures. We used a 12-W halogen lamp as the white light source. This unpolarized light was spatially filtered by a condense lens, an iris diaphragm, and a collimation lens. It was focused on a single array by using a 10× objective lens. To avoid the influence from other arrays, the beam size focused on the array was ~150 μm. This was accomplished by adjusting the aperture size of the diaphragm. The transmission light was then collected by another 10× objective lens and focused on a fiber cable (400-μm core). The transmission spectrum was taken by using a fiber-coupled linear charge-coupled device (CCD) array spectrometer (BWTEK and BTC112E).

Figure 2 shows the measured transmission spectra for three different kinds of nanostructures covered with water. There are transmission peaks and dips in the spectra due to the SPR effect. Equation 1 indicates that the SPR happens near the phase-matching conditions. In these periodic nanostructures, there are two interfaces (water/gold and water/glass) that can produce the SPR modes. For the zero-order mode, the SPR wavelength in water/gold interface is 824.83 nm ($\varepsilon_m = -29 + 2.0i$ for gold at 800 nm, $n = 1.332$ and $a_0 = 600$ nm). The SPR wavelength at glass/gold interface is 903 nm ($\varepsilon_m = -36 + 2.64i$ for gold at 900 nm wavelength, $n = 1.46$ and $a_0 = 600$ nm). From Fig. 2, it is seen that there are transmission dips near 825- and 900-nm wavelengths. These measured results indicate that the transmission near the phase-matching condition is a local minimum, not a maximum. The transmission peak occurs at a wavelength ~30 nm longer than the predictive SPR wavelength. For the water/gold interface, the maximum transmission is at ~865 nm wavelength. For the glass/gold interface, the transmission peak is at ~930 nm.

Figure 3 shows the transmission spectra of nanohole arrays and nanoslit arrays with different aperture sizes. The diameters of holes ranged from 108 to 236 nm. The slit
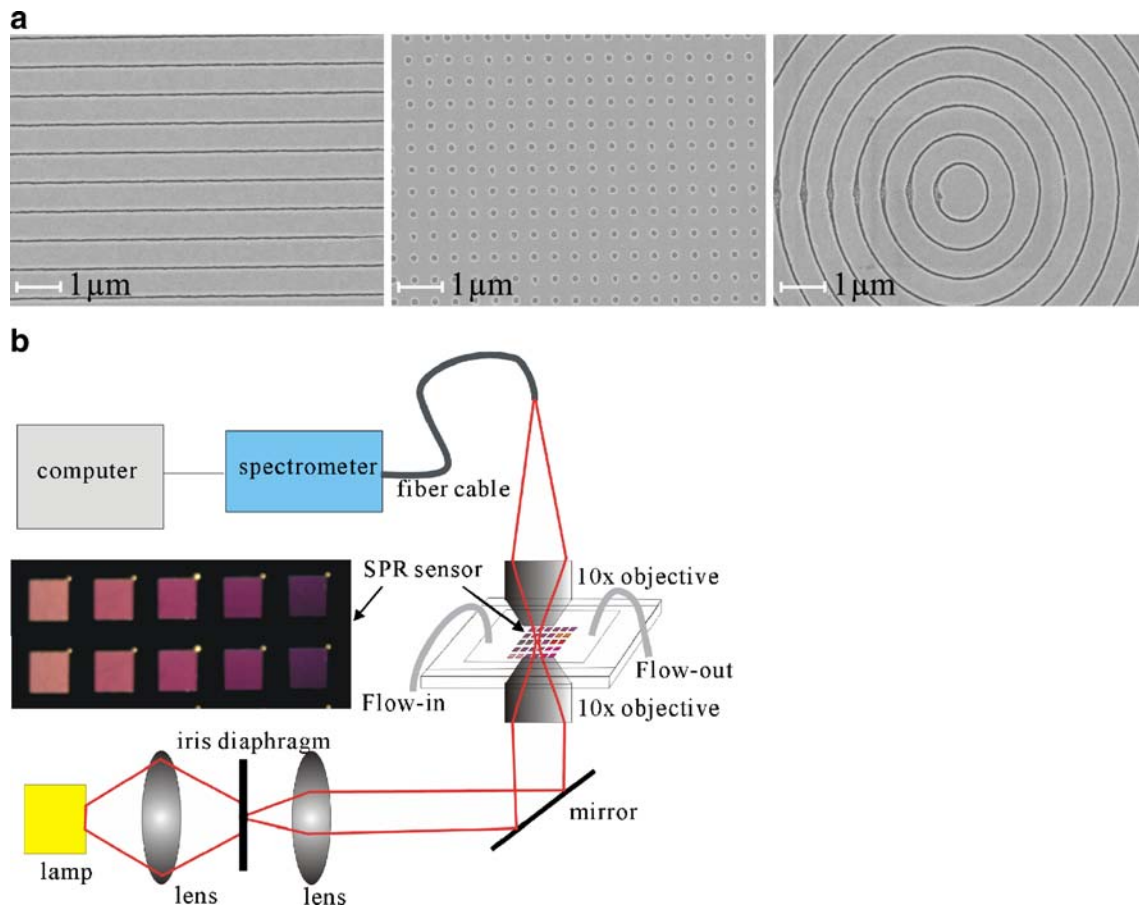
Fig. 1 The SEM images for different gold nanostructures on a glass substrate: **a** a nanoslit array, **b** a nanhole array, and **c** concentric circles. These arrays have the same 600-nm period and the same area of 150×150 μm. **b** The optical setup for transmission spectrum measurement. The light source was a halogen lamp. The iris diaphragm and 10×-objective lens made an optical spot ~150 μm on the sample surface. The transmission spectrum was taken by a linear CCD array spectrometer. The *inset* shows the transmission optical image of nanoslit arrays with slit widths ranging from 20 to 100 nm

gaps varied from 43 to 126 nm. These figures show that the SPR wavelength is changed with the aperture size. The SPR wavelength has a blueshift with the reduction of hole diameter. On the contrary, decreasing the slit gap results in a redshift of the SPR wavelength. For per nanometer decrease of the aperture, a nanohole array has a 0.26-nm blueshift in the peak wavelength, while a nanoslit array has only a 0.096-nm redshift. The aperture size seems to have a larger influence on the nanohole array than on the nanoslit array.

We interpret the above transmission spectra by using the Fano model, which describes the interaction of a continuum state and a zero-order discrete state [11]. In a periodic nanostructure, the continuum state is the isolated aperture excitation state, which could include contributions from localized surface plasmons [18]. The discrete state is the surface plasmon wave propagating in a periodic structure as described by the Bloch wave. Constructive and destructive
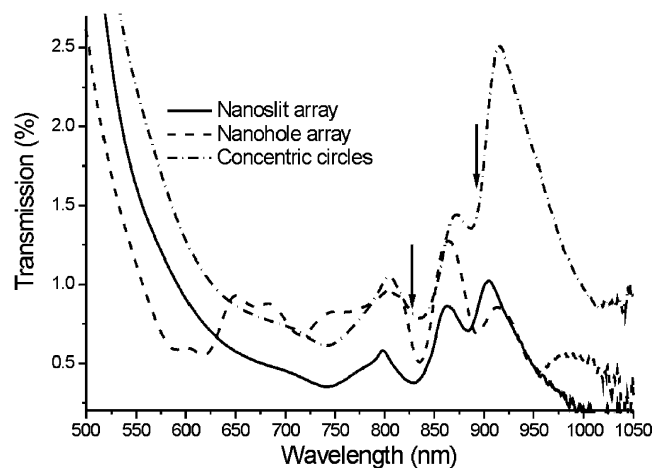
Fig. 2 The transmission spectra for different 600-nm-period nano-structures in water: a nanoslit array (slit width, ~70 nm), a hole array (hole size, ~150 nm), and concentric circles (line width, ~70 nm). The *arrows* indicate the wavelengths for the phase-matching conditions at water/gold and glass/gold interface

a

b

$Y=0.26X+815.383(nm)$

c

d

$Y=-0.09556X+870.169 \ (nm)$
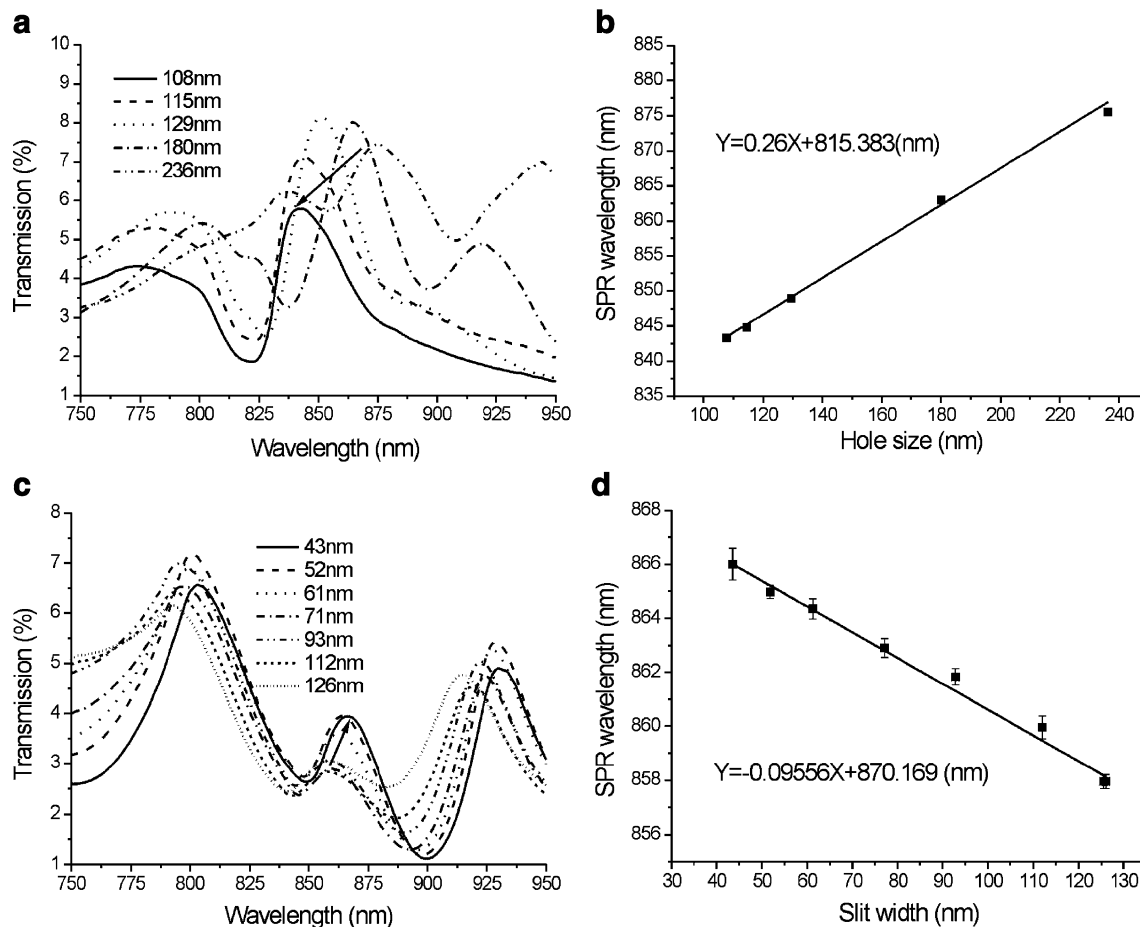
Fig. 3 The transmission spectra for **a** nanohole arrays and **c** nanoslit arrays with different sizes of apertures. The hole diameters ranged from 108 to 236 nm. The slit widths varied from 43 to 126 nm. Those arrays had the same 600-nm period and film thickness. **b** The wavelength shift vs. the hole diameter. **d** The wavelength shift vs. the slit width. For per nanometer increase of the aperture, the change in peak wavelength for a nanohole array is 0.26 nm and is only −0.096 nm for a nanoslit array

interference of these states leads to the Fano line shapes. The upper state position is associated with the transmission minimum and the lower state position with the transmission maximum. The lower state has lower photon energy. Hence, the transmission maximum has a redshift relative to the minimum. When the hole diameter or slit gap is changed, the continuum state (isolated hole/slit excitation) is also changed. For the nanoslit array, the TM polarized wave excites gap plasmons in the slits. The resonance of gap plasmons in the nanoslit results in the continuum state [19]. The decrease of slit gap increases the propagation constant of the gap palsmon [20]. As a result, the resonant wavelength is redshift. On the other hand, the nanohole array is subjected to the cut-off condition. As the hole size decreased, the decreased transmission will be less for shorter wavelengths than for larger wavelengths [21]. Therefore, the spectrum of continuum state is blueshifted with a decrease of hole diameter.

It is noticeable that the nanoslit array and concentric circles consisted of the same nanometer lines. Their aperture sizes are similar. However, the slit array is a one-dimensional structure. Only the TM wave can propagate in the nanoslits. The transverse-electric wave is under cut-off condition. Half of the incident light cannot contribute to the transmission. On the other hand, concentric circles are circularly symmetric. The normally incident wave can propagate without any cut-off. Therefore, its optical transmission is twice larger than that of a nanoslit array.

Sensitivity measurement

In most SPR biosensors, aqueous conditions are preferred. We thus tested the sensitivities of periodic nanostructures in water environment. Figure 4a shows the transmission spectra of a nanohole array covered with different methanol/water mixtures. There was an apparent redshift when the surface condition changed from water to a methanol-rich medium. Figure 4b shows the wavelength shift measured at transmission peak and dip as a function of
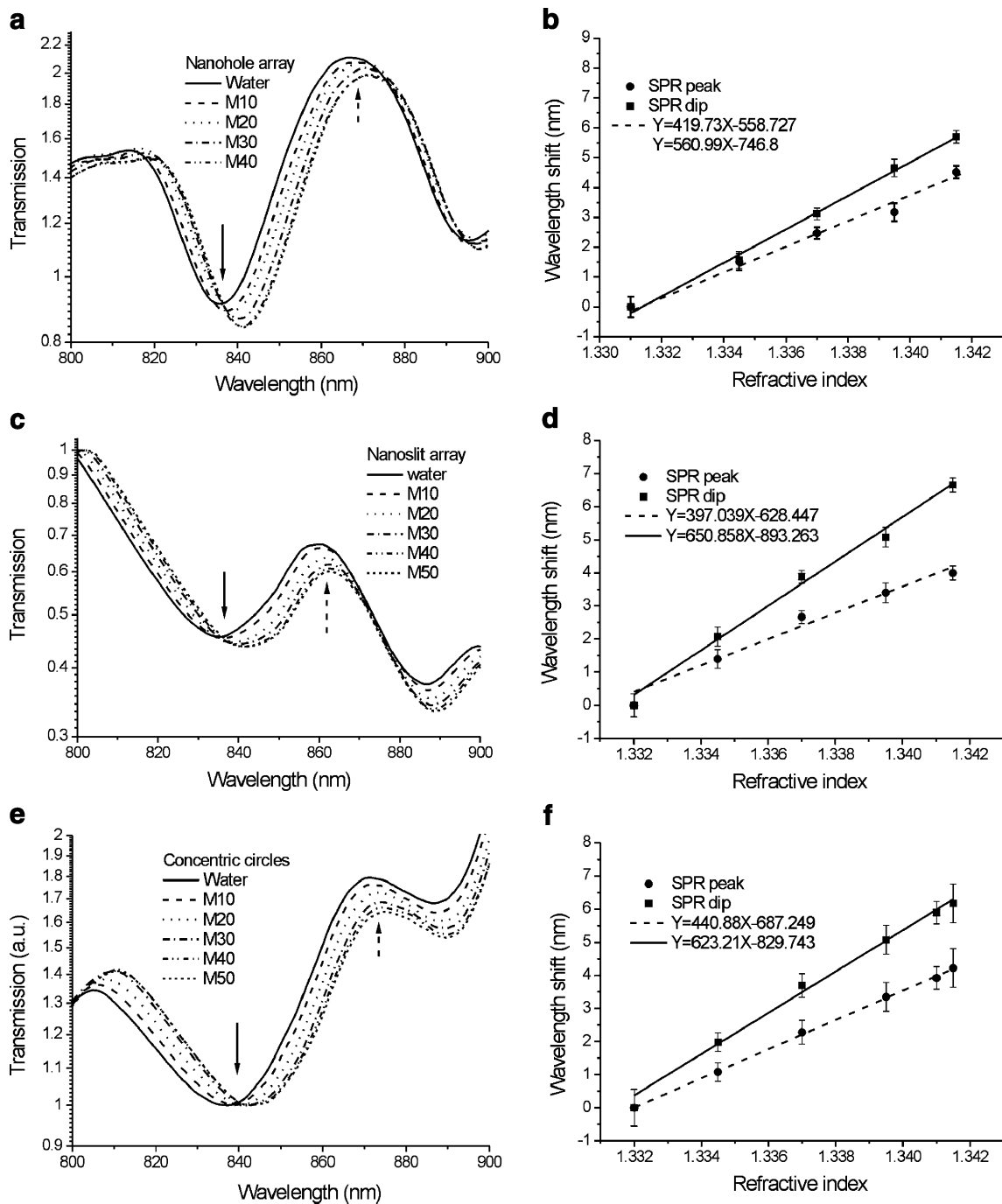
Fig. 4 **a** The transmission spectra of a nanohole array in water and different methanol/water mixtures. There was apparent redshift when outside medium changed from water to a methanol-rich medium, 10%, 20%, 30%, and 40% (*w/w*), respectively. **b** The wavelength shifts vs. the refractive index of surface medium. The slopes of the fitting curves show the wavelength sensitivity. It is ~560.99 nm/RIU for dip wavelength and is ~419.73 nm/RIU for peak wavelength. **c** The transmission spectra of a nanoslit array in different methanol/water mixtures. **d** The wavelength shifts against the refractive index of outside medium. The slopes show that the RIU sensitivity is 650.85 nm/RIU for dip wavelength and 397.04 for peak wavelength. **e** The transmission spectra of concentric circles in different methanol/water mixtures. **f** The wavelength shifts against the refractive index of outside medium. The slopes show that the RIU sensitivity is 623.21 nm/RIU for dip wavelength and 440.88 for peak wavelength

the refractive index of covered medium. The slopes of the fitting curves are the wavelength sensitivity. At the dip wavelength, the sensitivity is 560.99 nm/RIU. The sensitivity at the peak wavelength is only 419.73 nm/RIU,

similar with previous report [11]. From Eq. 2, the wavelength sensitivity for the fundamental mode ($i=1$, $j=0$ or $i=0$, $j=1$) is estimated as a_0 when $\varepsilon_m \gg n^2$. The theoretical sensitivity is ~600 nm/RIU for the 600-nm-
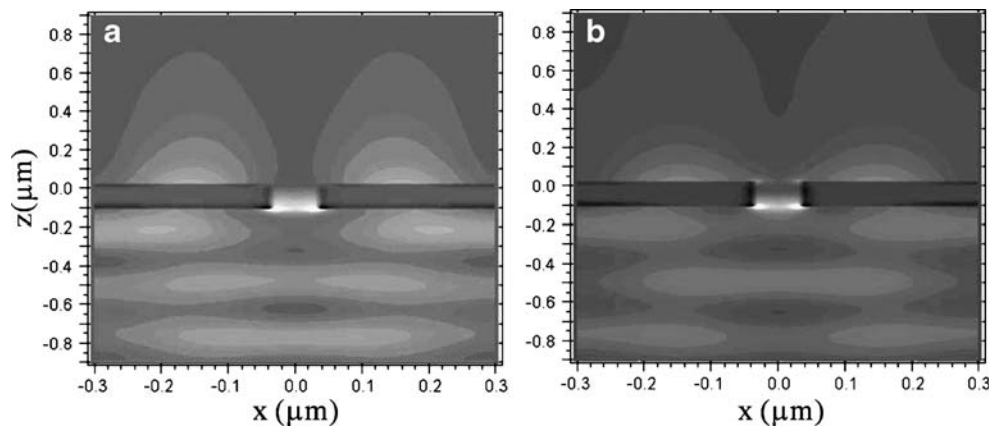
Fig. 5 The calculated distributions of optical intensity in a nanoslit array. The slit gap was 50 nm, the period was 600 nm, and the thickness of gold film was 110 nm. A TM-polarized wave was normally incident from the glass substrate. **a** The incident wavelength was 830 nm. The optical field shows that the surface plasmon wave stays in the metal film. **b** The incident wavelength was 860 nm. The optical field is intense near the slit edges and likely to couple out

period array. This value is close to the result measured at the dip wavelength. The value measured at peak wavelength is much smaller than the predicted value.

Figure 4c shows the transmission spectra of a nanoslit array in water and different methanol/water mixtures. It also shows an apparent redshift when outside medium changed from water to a methanol-rich medium. Figure 4d shows the wavelength shift measured at the peak wavelength for different outside refractive index. The slope of the fitting curve shows the sensitivity measured at the dip wavelength is 650.86 nm/RIU. This sensitivity is about 16% higher than that of a nanohole array. The sensitivity measured at peak wavelength is only 367.04 nm/RIU, much smaller than that measured at dip wavelength. Figure 4e shows the transmission spectra of the concentric circles in water and different methanol/water mixtures. Figure 4f shows the wavelength shift against the refractive index of the outside medium. The slope shows that the sensitivity is 623.21 nm/RIU at dip wavelength and 440.88 nm/RIU at peak

wavelength. The sensitivities of a nanoslit array and concentric circles are similar and better than that of a nanohole array.

We have performed some FDTD calculations to verify the sensitivity differences in the peak and dip wavelengths. Figure 5 show the calculated distributions of optical intensity, $\varepsilon|E^2|/2$, in a nanoslit array. The slit gap was 50 nm, the period was 600 nm, and the thickness of gold film was 110 nm. A TM-polarized wave was normally incident from the glass substrate. The incident wavelength was 830 nm for the dip transmission and 860 nm for the peak transmission. The steady state pattern shows that the surface plasmon wave stays in the metal film at the wavelength of the transmission dip (Fig. 5a) and is most intense near the slit edges at the wavelength of transmission peak (Fig. 5b). This qualitatively agrees with the Fano model, where at the higher bandgap edge (transmission minimum), the surface plasmon polariton–Bloch wave (SPP-BW) stays in the metal film. Its lifetime is long and less likely to couple to the outside. While
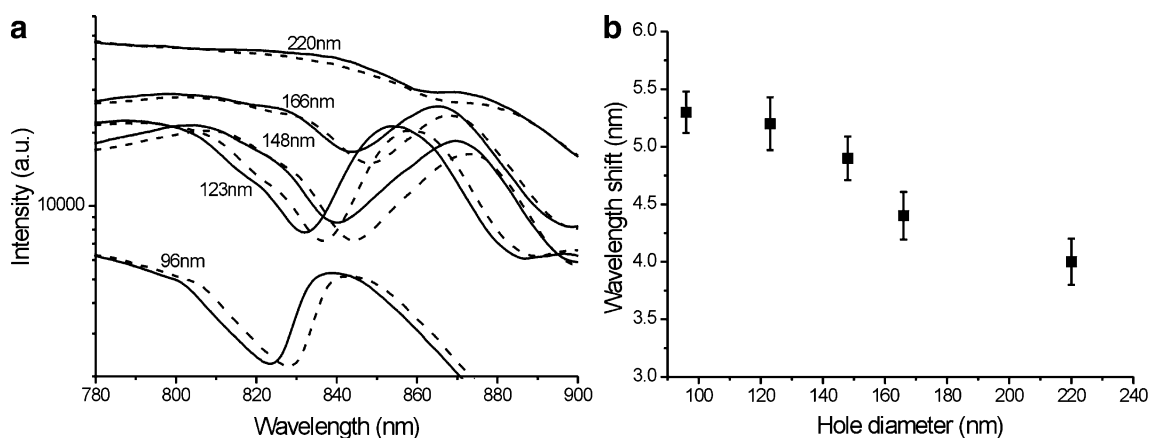
Fig. 6 a The transmission spectra of nanohole arrays with different hole diameters covered with water (*solid line*) and 40% methanol/water (*dash line*). **b** The wavelength shifts between water and 40% methanol/water mixture vs. the hole diameter. The sensitivity is decreased with the increase of hole diameter

for the lower bandgap edge (transmission maximum), the SPP-BW is short and likely to couple [13]. Because the SPR condition at dip wavelength is similar to a conventional long-range SPR, its sensitivity is thus close to the predicted value. At the peak wavelength, intense light is localized near the aperture edges. The short-range SPR results in a small sensitivity.

The effective metallic region where the SPR exists is an important parameter for the SPR mode sensitivity. In a nanoslit array, light is not cut off for a TM wave. The slit width is typically smaller than 100 nm. Therefore, metallic area of a nanoslit array is similar to a flat surface, yielding a sensitivity close to the predicted value. In a nanohole array, light is cut off when its diameter is smaller than one half of the incident wavelength. It limits the hole to a larger one to obtain detectable resonance. The hole diameter is typically larger than 100 nm. It reduces the effective metallic area for the SPR mode. To verify the effect of lateral resonant length on the RIU sensitivity, 600-nm-period nanohole arrays with different hole diameters from 96 to 220 nm were compared. Figure 6a shows the transmission spectra in water and 40% methanol/water, respectively. Figure 6b shows the wavelength shift between water and 40% methanol/water as a function of the hole diameter. It is obvious that the wavelength shift decreased with an increase of hole diameter. It decreased from 5.2 to 3.8 nm for 96- and 220-nm-diameter hole array, respectively. From the result, we concluded that the aperture size is important for the wavelength sensitivity of nanohole arrays.

In summary, surface plasmon mode sensitivities of gold nanoslit arrays, nanohole arrays, and concentric circles are studied in aqueous environment. Our measurement results suggest that high wavelength sensitivity is measured at the dip wavelength not at the peak wavelength. The possible reason is that long-range SPR occurs at the transmission dip, while intense short-range SPR is generated near the apertures at the transmission peak. The short-range SPR results in a lower sensitivity. It is also found that different types of nanostructures have different SPR sensitivities. A nanoslit array has a better sensitivity than a nanohole array because the effective metallic area of a nanoslit array is similar to a flat surface. The metallic area of a nanohole array is limited by the hole size due to the cutting off of light. Our measurement was taken in a small area of 150× 150 μm. The acquired time was shorter than 0.1 s. High-throughput and chip-based detections are feasible when thousands of arrays of periodic nanostructures can be fabricated on a glass chip.

References

1. Knoll W (1998) Annu Rev Phys Chem 49:569 doi:10.1146/annurev.physchem.49.1.569
2. Homola J, Yee SS, Gauglitz G (1999) Sens Actuators B Chem 54:3 doi:10.1016/S0925-4005(98)00321-9
3. Myszka DG, Rich RL (2000) Pharm Sci Technol Today 3:310 doi:10.1016/S1461-5347(00)00288-1
4. Ebbesen TW, Lezec HJ, Ghaemi HF, Thio T (1998) Nature 391:667 doi:10.1038/35570
5. Lezec HJ, Degiron A, Devaux E, Linke RA, Martin-Moreno L, Garcia-Vidal FL et al (2002) Science 297:820 doi:10.1126/science.1071895
6. Schröter U, Heitmann D (2000) Phys Rev B 58:15419 doi:10.1103/PhysRevB.58.15419
7. Brolo G, Gordon R, Leathem B, Kavanagh KL (2004) Langmuir 20:4813 doi:10.1021/la0493621
8. Stark PRH, Halleck AE, Larson DN (2005) Methods 37:37 doi:10.1016/j.ymeth.2005.05.006
9. Pang L, Hwang GM, Slutsky S, Fainman Y (2007) Appl Phys Lett 91:123112 doi:10.1063/1.2789181
10. Lee KL, Lee CW, Wang WS, Wei PK (2007) J Biomed Opt 12 (4):044023 doi:10.1117/1.2772296
11. Genet C, Van Exter MP, Woerdman JP (2003) Opt Commun 225:331 doi:10.1016/j.optcom.2003.07.037
12. Benabbas A, Halté V, Bigot JY (2005) Opt Express 13:8730 doi:10.1364/OPEX.13.008730
13. Chang SH, Gray S, Schatz G (2005) Opt Express 13:3150 doi:10.1364/OPEX.13.003150
14. Cao Q, Lalanne P (2002) Phys Rev Lett 88:057403 doi:10.1103/PhysRevLett.88.057403
15. Fan W, Zhang S, Minhas B, Malloy KL, Brueck RJ (2005) Phys Rev Lett 94:033902 doi:10.1103/PhysRevLett.94.033902
16. Klein Koerkamp KJ, Enoch S, Segerink FB, Van Hulst NF, Kuipers L (2004) Phys Rev Lett 92:183901 doi:10.1103/PhysRevLett.92.183901
17. Wei PK, Chou HL, Fann WS (2002) Opt Express 10:1418
18. Degiron A, Ebbesen TW (2005) J Opt A Pure Appl Opt 7:S90 doi:10.1088/1464-4258/7/2/012
19. Moreau A, Lafarge C, Laurent N, Edee K, Granet G (2007) J Opt A, Pure Appl Opt 9:165 doi:10.1088/1464-4258/9/2/008
20. Jung YS, Sun Z, Wuenschell J, Kim HK, Kaur P, Wang L et al (2006) Appl Phys Lett 88:243105 doi:10.1063/1.2209717
21. Van der Molen KL, Segerink FB, Van Hulst NF, Kuipers L (2004) Appl Phys Lett 85:4316 doi:10.1063/1.1815379